Noname manuscript No.
(will be inserted by the editor)

A sharp interface method using enriched finite elements for elliptic interface problems

Susanne Höllbacher · Gabriel Wittum

Received: date / Accepted: date

Abstract We present an immersed boundary method for the solution of elliptic interface problems with discontinuous coefficients which provides a second-order approximation of the solution. The proposed method can be categorised as an extended or enriched finite element method (XFEM). In contrast to other extended FEM approaches, the new shape functions get projected in order to satisfy the Kronecker-delta property with respect to the interface. The resulting combination of projection and restriction was already derived in [19] for application to particulate flows. The crucial benefits are the preservation of the symmetry and positive definiteness of the continuous bilinear operator. Besides, no additional stabilisation terms are necessary. Furthermore, since our enrichment can be interpreted as adaptive mesh refinement, the standard integration schemes can be applied on the cut elements. Finally, small cut elements do not impair the condition of the scheme and we propose a simple procedure to ensure good conditioning independent of the location of the interface. The stability and convergence of the solution will be proven and the numerical tests demonstrate optimal order of convergence.

Keywords elliptic interface problem · immersed boundary method · discontinuous coefficients · enriched finite elements · Petrov-Galerkin finite volumes

S. Höllbacher
King Abdullah University of Science and Technology (KAUST), Computer, Electrical and Mathematical Sciences and Engineering (CEMSE), Thuwal, 23955-6900, KSA
Goethe-Center for Scientific Computing (G-CSC), Johann Wolfgang Goethe University, Kettenhofweg 39, 60423 Frankfurt, Germany
E-mail: susanne.hoellbacher@gcsc.uni-frankfurt.de

G. Wittum
King Abdullah University of Science and Technology (KAUST), Computer, Electrical and Mathematical Sciences and Engineering (CEMSE), Thuwal, 23955-6900, KSA

1 Introduction

Many applications in engineering and biology involve immersed interfaces moving in time within the computational domain. Examples include electrostatics, heat conduction, diffusion problems and elasticity. The application of our interest is the motion of incompressible immiscible fluids.

Interface problems can be discretised using fitted or unfitted finite element spaces. In a fitted approach, the variational formulation is based on the continuous bilinear form and therefore inherits all its properties. Especially stability and optimal order of convergence can be guaranteed. However, in case of moving interfaces, the mesh generation process becomes expensive.

In order to avoid expensive re-meshing the immersed boundary method (IBM) has become a popular method to ease the representation of the geometry by allowing the interface to cut the elements. The original IBM was formulated by Peskin [28] for fluid-structure interactions. New *Lagrangian points* (LP) are defined along the interface. Since the singular forces arising at the interface can be understood as delta functions, Peskin introduces suitable discrete delta functions (DDF) for the Lagrangian degrees of freedom which spread the forces into the surrounding domain. The discontinuity will be smoothed out and therefore one drawback is a minor accuracy. In [30] and [31] a generalized IBM with higher order approximation is developed. The discrete delta function acts as a link between the moving interface and fixed Eulerian grid. Since it employs explicit expressions for the body force, it is categorized into the class of *direct forcing* schemes and can be interpreted as fitted method. A good overview is given in [25].

An alternative approach are unfitted finite elements. As for the IBM of Peskin, the Eulerian mesh does not resolve the interface. By introducing local modifications, enrichments or extensions of the finite element spaces, the features of the interface can be approximated properly. The most prominent example is the extended finite element method (XFEM) first introduced by Moës et al. [26] to model the discontinuities without adapting the grid to the interface. In [29] and [13] XFEM is applied to flow problems in order to model the discontinuity of the pressure. In the recent work of Kirchhart et al. [22] theoretical analysis of the XFEM is applied to the interface Stokes problem. Other developements include the generalized finite element method [21] and the unfitted Nitsche method by Hansbo and Hansbo [15], also called *cut finite element method* (CutFEM). In contrast to the early XFEM approaches slightly different enrichment functions are utilised for the description of the discontinuity at the interface and Nitsche's method, cf. [27], is applied to impose the interface conditions weakly. Further penalty terms need to be introduced to stabilize the system. CutFEM was first derived for the elliptic interface problem by Hansbo and Hansbo [15], later Becker et al. [3] and Hansbo et al. [17] developed the method for a Stokes interface problem and in [16], [6] the weak coupling approach was applied to fluid-structure interaction. In [6] the problem of pressure oscillation at the interface is treated by introducing penalty terms. A drawback of these methods is that the structure of the operators

becomes more complicated due to additional enrichment. Furthermore, some enrichments produce ill-conditioning due to "small" cut elements for which the volume on one of the parts of the cut element gets very small and equally the support of the associated shape function. Additional penalisation terms yields operators which differ from the original elliptic operator. Since in the literature the terms XFEM and CutFEM are not perfectly distinguishable we will use the term CutFEM because we mainly refer to the extended finite element spaces as defined in [15]. One focus of this article is the comparison of differently modified local finite element spaces.

The immersed boundary method derived in this work lies in-between fitted and unfitted methods. After enriching and modifying the local finite element spaces in a proper way the proposed spaces on cut elements are conforming to the interface. This resembles an enrichment by discrete delta-like functions. But in contrast to Peskins approach they can be embedded into the function space of the Eulerian mesh. The result is a fitted method and the essential benefit of the enrichment is that desireable porperties of the continuous bilinear form like symmetry and positive definiteness are preserved. In particular, stability results can be derived easily without the necessity to introduce additional penalisation terms. Furthermore, our enrichment can be interpreted as a standard Galerkin scheme on an adaptively refined mesh. This perspective enables to apply the standard integration schemes which simplifies the assembling procedure on cut elements. Finally, a good condition of the discrete system can be provided by slight changes dependent on the location of the interface. But in contrast to other extended methods, where the conditioning is impaired on small cut elements, our enriched spaces features a natural stabilisation on cut elements with small support of the shape function. Our derived enrichment can be summarized as *projection* onto a space which inherits the interface under the condition to form a *partition of unity* (PU) which yields a *reduction* of the shape functions surrounding the interface. The *projection* and the *reduction* are therefore the key ingredients of the proposed immersed boundary method.

In an earlier work, c.f. [19], the construction of the proposed enrichment spaces were derived via a *vertex-centered* finite volume method (FVM). For the formulation of a vertex-centered FV (finite volume element method, box method) usually a second, dual mesh is introduced. Using first-order trial functions on the primal mesh (given triangulation) and piecewise constant test functions on the corresponding dual mesh the FV scheme can be formulated in variational form (Petrov-Galerkin method). Therefore we will further refer to it as a *Petrov-Galerkin* finite volume method (PG-FVM). Expoliting the Petrov-Galerkin interpretation of this method enables the development of the associated enriched finite element scheme. As a consequence, our method is applicable to FE schemes and to *vertex-centered* FV schemes. It should be emphasized that another common FV discretisation, the so-called *cell-centered* FV scheme, follows another approach. The technique which will be derived in this paper refers to the vertex-centered scheme. Since one focus of this article is the comparison of differently modified local finite element spaces, we emphasize

that also the DDF can be interpreted as an extension of the function spaces used for the approximation of the solution.

The paper is organized as follows: In Section 2 we introduce the enriched spaces for a general elliptic interface problem of diffusion with discontinuous coefficients, since it likewise reflects many interface problem of interest. A suitable finite element (projFEM) and finite volume scheme (projFVM) will be derived. In Section 3 we compare the spaces with those of CutFEM and DDF-IBM. In Section 4 the properties of the enriched spaces are described in more detail. In Section 5 consistency, symmetry, stability and convergence of the scheme are proven. Finally, we present numerical results in Section 6 for the projFVM.

2 Mathematical Formulation

For the formulation of our immersed boundary method we consider the elliptic equation with discontinuous coefficients

$$\begin{aligned} -\nabla \cdot (\alpha \nabla u) &= f && \text{in } \Omega_1 \cup \Omega_2, && (1)\\ [\alpha \nabla u \cdot \mathbf{n}] &= g && \text{on } \Gamma, && (2)\\ [u] &= 0 && \text{on } \Gamma, && (3)\\ u &= 0 && \text{on } \partial\Omega, && (4) \end{aligned}$$

on a polygonal and convex domain $\Omega := \Omega_1 \cup \Omega_2 \cup \Gamma \subset \mathbb{R}^d$ with embedded, sufficiently smooth interface $\Gamma = \partial\Omega_1 \cap \partial\Omega_2$. The jump condition on Γ is given by $[\alpha \nabla u \cdot \mathbf{n}] := (\alpha_1 \nabla u_1 - \alpha_2 \nabla u_2) \cdot \mathbf{n}$ with normal vector $\mathbf{n}$ on Γ pointing from Ω_1 to Ω_2. We assume $\alpha_j > 0$ to be constant in each subdomain Ω_j, $j = 1, 2$. We want to emphasize that, with regard to the applications of interest, we focus on moderate jumps of the coefficients. Additional treatment might be necessary for $\alpha_1/\alpha_2 \ll 1$ or $\gg 1$. Furhter, we assume that the interface is sufficiently resolved by the mesh. In [29], [7] and [15] different assumptions are stated to similarly assure this property.

With the standard Sobolev spaces $H^k(\Omega)$ and $H^k_0(\Omega)$ with norm $\|\cdot\|_{k,\Omega}$ we formulate the weak formulation as follows: Find $u \in H^1_0(\Omega)$ s.t.

$$a(u, v) = (f, v)_{0,\Omega} + (g, v)_{0,\Gamma} \qquad \forall\, v \in H^1_0(\Omega). \tag{5}$$

with bilinear form $a(u, v) := (\alpha \nabla u, \nabla v)_{0,\Omega}$ with respect to the coefficient α and standard $L^2(\Omega)$ scalar product $(\cdot, \cdot)_{0,\Omega}$.

We further introduce the Sobolev space of functions

$$H^2(\Omega_{1,2}) := \{v \in H^1_0(\Omega) \ : \ v|_{\Omega_i} \in H^2(\Omega_i),\, i = 1, 2\}$$

and according norm

$$\|\cdot\|^2_{2,\Omega_1 \cup \Omega_2} := \|\cdot\|^2_{2,\Omega_1} + \|\cdot\|^2_{2,\Omega_2}.$$

Assumig $f \in L^2(\Omega)$ and $g \in H^{1/2}(\Gamma)$ the problem (5) has a unique solution $u \in H^2(\Omega_{1,2})$, see [15]. In the next section we shall introduce appropriate discrete spaces to solve (5).

In [19] we derived an enrichment of the finite element spaces on cut elements which yields conforming finite elements w.r.t. the interface. Therein the scheme was applied to particulate flows. For this application the correct discretisation of the *forces* as a vectorial measure acting at the particle interface is crucial. The main motivation therefore was the consistency of the *gradients* of the shape functions instead of the their *values*. In this paper, we want to apply this gradient-consistent enrichment to the simpler Laplace equation with embedded interface. For this application, the second feature of the projected spaces being a fitted enrichment will be more important. We also compare the proposed enrichement with the extended spaces of the CutFEM and the DDF-IBM of Peskin.

2.1 Locally enriched finite element spaces

We will derive a *conforming* finite element formulation of the interface problem already defined for the application to particulate flows in [19]. Therefore, we define enriched spaces on the elements cut by the interface.

We first introduce some notations for quantities related to the mesh and the immersed interface. Let $\mathcal{T}_h$ be a shape-regular, simplicial triangulation of Ω and $\Gamma \subset \Omega$ the interface which usually does not coincide with the boundary of the elements of $\mathcal{T}_h$. Let $\mathcal{X}_{h,\Gamma} := \bigcup_{T\in\mathcal{T}_h} \partial T \cap \Gamma$ be the set of all intersecting points of Γ with the edges of elements. The (d-1)-dimensional convex hull of all points of $\mathcal{X}_{h,\Gamma}$ yields a piecewise planar approximation Γ_h of Γ. Let further $\Omega_{1,h}$ and $\Omega_{2,h}$ be the corresponding subdomains of Ω satisfying $\partial\Omega_{1,h} \cap \partial\Omega_{2,h} = \Gamma_h$. We introduce the set of all *cut elements* $\mathcal{T}_{h,\text{Cut}} := \{T \in \mathcal{T}_h \ : \ T \cap \Gamma \neq \emptyset\}$. By means of $\Omega_{1,h}$ and $\Omega_{2,h}$ all cut elements $T \in \mathcal{T}_{h,\text{Cut}}$ can be decomposed into the parts lying on either side of Γ_h, i.e. $\mathcal{T}^1_{h,\text{Cut}} := \{T \cap \Omega_{1,h} \ : \ T \in \mathcal{T}_{h,\text{Cut}}\}$ and $\mathcal{T}^2_{h,\text{Cut}} := \{T \cap \Omega_{2,h} \ : \ T \in \mathcal{T}_{h,\text{Cut}}\}$, respectively (see Fig. 2). Based on the sub-elements of $\mathcal{T}^1_{h,\text{Cut}}$ and $\mathcal{T}^2_{h,\text{Cut}}$ we define the new grid

$$\mathcal{T}^*_h := (\, \mathcal{T}_h \setminus \mathcal{T}_{h,\text{Cut}} \,) \cup \mathcal{T}^1_{h,\text{Cut}} \cup \mathcal{T}^2_{h,\text{Cut}}.$$

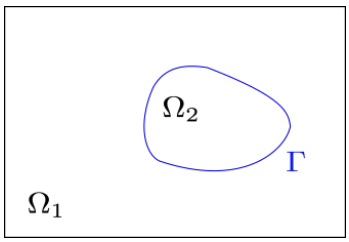

Fig. 1: Computational domain with embedded interface Γ.

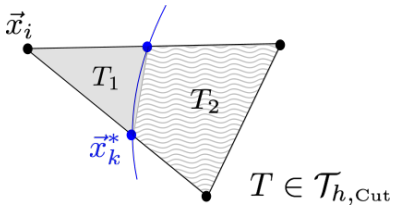

Fig. 2: Cut element $T = T_1 \cup T_2$: $T_1 \in \mathcal{T}^1_{h,\mathrm{Cut}}$, $T_2 \in \mathcal{T}^2_{h,\mathrm{Cut}}$, $\mathbf{x}^*_k \in \mathcal{X}_{h,\Gamma}$, $\mathbf{x}_i \in \mathcal{X}^1_{h,\mathrm{Cut}}$.

$\mathcal{T}_h^*$ can be interpreted as a special non-regular refinement of $\mathcal{T}_h$ with respect to Γ.

In order to construct appropriate function spaces we further introduce some notations for the different set of vertices. Let $\mathcal{X}_h$ and $\mathcal{X}_h^*$ be the set of all vertices of $\mathcal{T}_h$ and $\mathcal{T}_h^*$, respectively, and $\mathcal{X}_{h,\mathrm{Cut}}$ the vertices of all cut elements. The set of vertices $\mathcal{X}_{h,\mathrm{Cut}}$ can be decomposed into the set $\mathcal{X}_{h,\Gamma}$ of vertices on Γ_h and those being part of $\mathcal{X}_h$ and belonging to either side Ω_j, $j = 1, 2$, of the interface. This yields $\mathcal{X}_{h,\mathrm{Cut}} = \mathcal{X}_{h,\Gamma} \cup \mathcal{X}^1_{h,\mathrm{Cut}} \cup \mathcal{X}^2_{h,\mathrm{Cut}}$, with *near-interface vertices* $\mathcal{X}^j_{h,\mathrm{Cut}} := \{\mathbf{x} \in \mathcal{X}_{h,\mathrm{Cut}} \setminus \mathcal{X}_{h,\Gamma} \ : \ \mathbf{x} \in \Omega_j\}$, $j = 1, 2$. By numbering all vertices of the refined mesh $\mathcal{T}_h^*$ we can assign indices to different subgroups in accordance to the described groups of vertices. Following the notations for the vertices we denote the corresponding set of indices by $\mathcal{I}_h$, $\mathcal{I}_h^*$, $\mathcal{I}_{h,\mathrm{Cut}}$, $\mathcal{I}_{h,\Gamma}$, $\mathcal{I}^1_{h,\mathrm{Cut}}$ and $\mathcal{I}^2_{h,\mathrm{Cut}}$. This yields for example $\mathcal{I}_h \subset \mathcal{I}_h^*$. For comprehensive notation we equip the additional vertices on the interface Γ_h with a star, i.e. $\mathcal{X}_{h,\Gamma} = \{\mathbf{x}^*_k\}_{k \in \mathcal{I}_{h,\Gamma}}$, see Fig. 2.

Following standard finite element theory we define a basis $\{\varphi_i\}_{i \in \mathcal{I}_h}$ of nodal functions φ_i on $\mathcal{T}_h$ satisfying $\varphi_i(\mathbf{x}_j) = \delta_{ij}, \mathbf{x}_j \in \mathcal{X}_h$. Let $\mathcal{V}_h$ denote the according finite element space. For φ_i being the piecewise linear functions with respect to $\mathcal{T}_h$ it is $\mathcal{V}_h = \mathcal{P}^1(\mathcal{T}_h)$. Based on $\mathcal{T}_h^*$ we can similarly define a nodal basis $\{\varphi_i^*\}_{i \in \mathcal{I}_h^*}$. The resulting *enriched* finite element space will be denoted by $\mathcal{V}_h^*$. It should be noted that $\mathcal{T}^1_{h,\mathrm{Cut}}$ and $\mathcal{T}^2_{h,\mathrm{Cut}}$ will contain not only triangles or tetrahedrons, but also quadrilaterals or hexahedrons, prisms and pyramids, respectively (see Section 4.3 for a detailed description of considered elements). As a consequence, the enriched space $\mathcal{V}_h^*$ on $\mathcal{T}_h^*$ will contain not only linear but also multi-linear shape functions.

Remark 1 (Non-extended enrichment of finite element spaces) We emphasize that the described enrichment does *not* lead to an extension of the domain across the boundary, since it introduces the degrees of freedom *on* the interface.

2.2 projFEM: A conforming finite element formulation of the interface conditions

We define a slightly adapted coefficient $\alpha_h|_{\Omega_{j,h}} := \alpha_j$, $j = 1, 2$. In the case of the piecewise constant coefficient $\alpha_h(\mathbf{x})$ the finite element bilinear form $a_{\text{FE}}(u, v) : \mathcal{V}_h^* \times \mathcal{V}_h^* \to \mathbb{R}$ of the left hand side of (1) reads

$$a_{\text{FE}}(u, v) := (\alpha_h \nabla u, \nabla v).$$

We can directly write down the *projected* FEM (projFEM) as follows: Find $u \in \mathcal{V}_h^*$ s.t.

$$a_{\text{FE}}(u, v) = (f_h, v) + (g, v)_\Gamma \qquad \forall\, v \in \mathcal{V}_h^*, \tag{6}$$

with linear operators

$$(f_h, v) := \int_\Omega f_h\, v\, d\mathbf{x} \qquad \text{and} \qquad (g, v)_\Gamma := \int_\Gamma g\, v\, d\mathbf{s}, \qquad v \in \mathcal{V}_h^*.$$

Let f_h on $\Omega_{j,h}$ be some appropriate approximation to f on Ω_j, $j = 1, 2$, satisfying $|\,(f, v_h) - (f_h, v_h)\,| \leq Ch \,\|\, v_h \,\|_{0,\Omega_1 \cup \Omega_2}$ for all $v_h \in \Pi(\mathcal{V}_h^*)$. In contrast to α_h the interface condition $(g, v_h)_\Gamma$ will be evaluated along the original interface Γ and not be replaced by Γ_h. The resulting finite element scheme is a Galerkin formulation on the entire domain Ω with respect to the enriched space $\mathcal{V}_h^*$ and additional right hand side $(g, v)_\Gamma$. We emphasize that testing with $\varphi_k^* \in \mathcal{V}_h^*$ with $k \in \mathcal{I}_{h,\Gamma}$ yields the following *kind-of-weak* form of the interface condition (2):

$$a_{\text{FE}}(u, \varphi_k^*) = \int_\Omega \alpha_h \nabla u \cdot \nabla \varphi_k^*\, d\mathbf{x} = (f_h, \varphi_k^*) + (g, \varphi_k^*)_\Gamma, \qquad k \in \mathcal{I}_{h,\Gamma}. \tag{7}$$

2.3 projFVM: A conforming finite volume formulation of the interface condition

We now apply the enriched space $\mathcal{V}_h^*$ in order to solve the interface problem in the PG-FV formulation. In [19] we proceeded in inverse direction and started with the vertex-centered PG-FV formulation in order to derive the enriched finite element spaces. This illustrates nicely, that because of their close relation either direction can be appropriate, depending on the purpose and application.

Choosing different trial and test spaces yields so-called *Petrov-Galerkin* schemes. The choice of piecewise constant test functions introduces additional boundary integrals in the weak formulation (as in the context of DG schemes). As a consequence, the resulting Petrov-Galerkin scheme is a finite volume formulation balancing along the according boundaries. Application of the enriched space $\mathcal{V}_h^*$ finally yields the following projected finite volume formulation (projFVM): Find $u \in \mathcal{V}_h^*$ s.t.

$$a_{\text{FV}}(u, v) = (f_h, v) + (g, v)_\Gamma \qquad \forall\, v \in \overline{\mathcal{V}}_h^*, \tag{8}$$

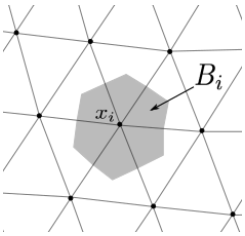

Fig. 3: Vertex-centered PG-FVM (*box method* [1]) with *barycentric* control volume B_i associated to the vertex $\mathbf{x}_i$.

with bilinear form

$$a_{\mathrm{FV}}(u,v) := -\sum_{i\in\mathcal{I}_h^*}\int_{\partial B_i} \alpha_h \nabla u\cdot\mathbf{n}\, v\, d\mathbf{s},$$

a set of so-called *control volumes* $\mathcal{B}_h^* := \{B_i^*\}_{i\in\mathcal{I}_h^*}$ and the function space of piecewise constants on each control volume $B_i^* \in \mathcal{B}_h^*$ defined as

$$\overline{\mathcal{V}}_h^* := \{v\in\mathcal{P}^0(\mathcal{B}_h^*)\ :\ v|_{\partial\Omega}=0\,\}.$$

The control volumes w.r.t $\mathcal{T}_h$ will be denoted by B_i accordingly. We emphasize that for a given simplicial mesh $\mathcal{T}_h$ the set $\mathcal{B}_h$ is required to form a partition of the domain Ω, but not necessarily is a simplicial decomposition or even identical with $\mathcal{T}_h$. In the case of the vertex-centered PG-FVM used in this work each B_i is constructed around the vertex $\mathbf{x}_i \in \mathcal{T}_h$ by connecting the barycenters of all neighbouring edges, faces and volumes to a convex hull enclosing $\mathbf{x}_i$ (see Fig. 3). The indicator functions $\chi_i(\mathbf{x})|_{B_i} \equiv 1$, $\chi_i(\mathbf{x}) \equiv 0$ else, for all $B_i \in \mathcal{B}_h$ form a basis of the test space $\overline{\mathcal{V}}_h$ and by construction we can define a bijective mapping $\mathit{\Pi} : \mathcal{V}_h \to \overline{\mathcal{V}}_h$, $\mathit{\Pi}(\varphi_i) := \chi_i$ between the basis of the Galerkin and Petrov-Galerkin test spaces. Analogously, we can define the mapping $\mathit{\Pi} : \mathcal{V}_h^* \to \overline{\mathcal{V}}_h^*$, $\mathit{\Pi}(\varphi_i^*) := \chi_i^*$ between the enriched test spaces. The standard control volumes related to the original mesh $\mathcal{T}_h$ are depicted in Fig. 4a and those with respect to $\mathcal{T}_h^*$ in Fig. 4b. We emphasize that for $\mathbf{x}_i \in \mathcal{X}_{h,\mathrm{Cut}}^j \subset \mathcal{X}_h$, $j = 1, 2$, the support of the according shape functions φ_i^* gets *reduced* to the cut parts $\mathcal{T}_{h,\mathrm{Cut}}^j$, $j = 1, 2$ of an element and therefore the related B_i^* gets *reduced* accordingly (compare the colored control volumes in Fig. 4a and in 4b). Consequently, the partition $\mathcal{B}_h^*$ contains the additional *interface-enclosing* control volumes B_k^* associated to the additional vertices $\mathbf{x}_k^* \in \mathcal{X}_{h,\mathit{\Gamma}}$ satisfying $\mathit{\Gamma}\cap B_i \neq \emptyset$, as depicted shaded in grey in Fig. 4b. By means of the bijective mapping $\mathit{\Pi}$ it is

$$\dim(\,\mathit{\Pi}(\mathcal{V}_h^*)\,) = \dim(\,\mathcal{V}_h^*).$$

Consequently, the enrichment by the grey control volumes is compatible with the enrichment $\mathcal{V}_h^*$ of the finite element test space. We can interpret the space

of piecewise constant functions $\Pi(\mathcal{V}_h^*)$ as the *enriched test space* for the PG-FVM with respect to the interface Γ.

In analogy to (7) we can state: Testing with $\chi_k^* \in \Pi(\mathcal{V}_h^*)$ with $k \in \mathcal{I}_{h,\Gamma}$ yields the following *kind-of-weak* form of the interface condition (2):

$$a_{\text{FV}}(u, \chi_k^*) = \int_{\partial B_k^*} \alpha_h \nabla u \cdot \mathbf{n} \, d\mathbf{s} = (f_h, \chi_k^*) + (g, \chi_k^*)_\Gamma \qquad k \in \mathcal{I}_{h,\Gamma}. \tag{9}$$

Therefore, the pointwise interface condition (2) is replaced by equilibrated fluxes across the boundary of the control volume B_k^*, enclosing the part $\Gamma \cap B_k^*$ of the interface, as depicted in Fig. 4b

2.4 Relating the Galerkin FEM and the PG-FVM

For the special choice of control volumes as drawn in Fig. 3 the resulting Petrov-Galerkin scheme is known to satisfy

$$\int_{\partial B_i \cap T} \nabla u \cdot \mathbf{n} \, d\mathbf{s} = -\int_T \nabla u \cdot \nabla \varphi_i \, d\mathbf{x}, \tag{10}$$

on all simplicial elements $T \in \mathcal{T}_h^*$ with accordingly piecewise linear functions $u, \varphi_i \in \mathcal{P}^1(\mathcal{T}_h^*)$ and normalized test function $\varphi_i(\mathbf{x}_i) = 1$. This identity was first proven by Bank and Rose [1] for the two-dimensional case and later also for arbitrary dimension by Chen [8], Xu and Zou [35] and Hackbusch [14]. Therefore, for piecewise linear spaces on simplices it reproduces the stiffness matrix for the Laplace (assuming piecewise constant coefficients on each triangle). We write down the following, generalized identification between $a_{\text{FE}} : \mathcal{V}_h^* \times \mathcal{V}_h^* \to \mathbb{R}$ and $a_{\text{FV}} : \mathcal{V}_h^* \times \Pi(\mathcal{V}_h^*) \to \mathbb{R}$:

$$a_{\text{FE}}(u, v) = a_{\text{FV}}(u, \Pi(v)) + \mathsf{Rest}(h) \qquad \forall\, u,\, v \in \mathcal{V}_h^*, \tag{11}$$

with $\mathsf{Rest}(h) = 0$ due to (10) in the case of the original, simplicial mesh $\mathcal{T}_h$. In [36] the estimate $\mathsf{Rest}(h) = O(h^2)$ was derived for rectangular meshes. The only requirement is an approximation of $\alpha(\mathbf{x})$ by a piecewise constant representation. In the works of Ye [36] and Chou and Kwak [9] that strong relation serves for the analysis of finite volume schemes for the Stokes equations. In [20] and [19] we similarly exploited this identification for the formulation of the FEM for particulate flow.

The identification (11) then yields $a_{\text{FE}}(u, \varphi^i) \approx a_{\text{FV}}(u, \chi_i)$ for all $i \in \mathcal{I}_h^*$ and with regard to (7) and (9) we can particularly state for all $k \in \mathcal{I}_{h,\Gamma}$ that

$$\int_{\omega_k} \alpha_h \nabla u \cdot \nabla \varphi_k^* \, d\mathbf{x} \approx \int_{\partial B_k^*} \alpha_h \nabla u \cdot \mathbf{n} \, d\mathbf{s} \qquad k \in \mathcal{I}_{h,\Gamma},$$

with equality on simplicial elements. In other words, testing on a *volume* by integrating on the support $\omega_k := \text{supp}(\varphi_k^*)$, $k \in \mathcal{I}_{h,\Gamma}$ can be replaced by balancing along a *surface* by integrating along the boundary ∂B_k^* of that special

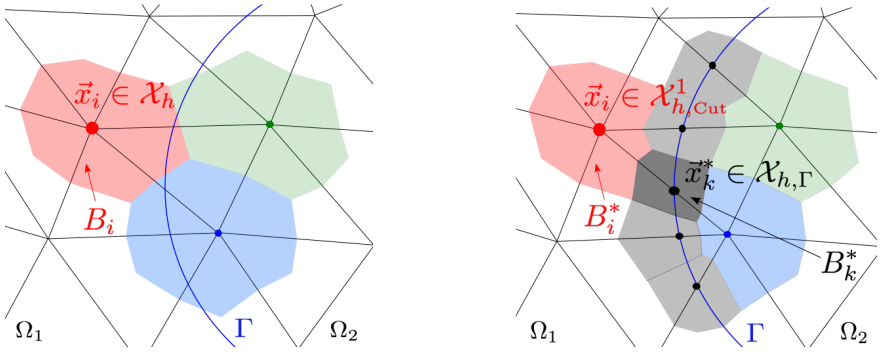

(a) Control volumes w.r.t. $\mathcal{T}_h$.

(b) Control volumes w.r.t. $\mathcal{T}_h^*$.

Fig. 4: Barycenter control volumes (a) for the original triangulation $\mathcal{T}_h$ and (b) for the enriched triangulation $\mathcal{T}_h^*$. It is $B_i = \mathrm{supp}(\mathit{\Pi}(\varphi_i))$ for $\mathbf{x}_i \in \mathcal{X}_h$, $B_i^* = \mathrm{supp}(\mathit{\Pi}(\varphi_i^*))$ for $\mathbf{x}_i \in \mathcal{X}^1_{h,\mathrm{Cut}}$ and $B_k^* = \mathrm{supp}(\mathit{\Pi}(\varphi_k^*))$ for $\mathbf{x}_k^* \in \mathcal{X}_{h,\mathit{\Gamma}}$.

interface-enclosing control volumes of the PG-FVM in (8). We emphasize the relation $B_k^* \subset \omega_k$.

We want to mention the slight difference in the right hand sides in (7) compared to (9). For simplicial meshes we get identity of the right hand sides for $f \in \mathcal{P}^0(\mathcal{T}_h)$, see e.g. [4], but in general both may differ.

Due to the construction of $\mathbf{x}_k^* \in \mathcal{X}_{h,\mathit{\Gamma}}$ the associated B_k^* in particular satisfy the relation

$$\mathit{\Gamma} \subset \bigcup_{k \in \mathcal{I}_{h,\mathit{\Gamma}}} B_k^*,$$

independent of the original grid $\mathcal{T}_h$, see also Fig. 4b. Finally, condition (3) is satisfied as well, since the shape functions φ_k^*, $k \in \mathcal{I}_{h,\mathit{\Gamma}}$ are continuous across the interface. We emphasize that their gradients have a jump along the *discrete* interface $\mathit{\Gamma}_h \cap B_k^*$, not along $\mathit{\Gamma}$ and together with the adaption of α_h the solution inherits the discontinuous gradient across $\mathit{\Gamma}_h$ instead of $\mathit{\Gamma}$. In Section 5 we prove that these adaptions are still consistent.

3 Comparison of projFEM/projFVM with CutFEM and DDF-IBM

Since the immersed boundary method derived in this work shares ideas of the IBM by Peskin [28] as well as the extended finite element techniques of CutFEM we will compare the according function spaces. First, we emphasize the following: A DDF-IBM introduces new nodes into the system. But since explicit expressions of the boundary conditions are formulated as force terms, these nodes are not treated as independent degrees of freedom. In contrast, XFEM techniques as CutFEM introduce additional shape functions on the cut elements and thereby new degrees of freedom. Since the shape functions

are commonly defined w.r.t. the underlying Eulerian grid, the new degrees of freedom are *not* located directly on the immersed interface but the domain gets extended across the interface. Main motivation of both strategies is to maintain the standard discretisation scheme on the background mesh.

For a proper comparison with CutFEM and DDF-IBM we construct the enriched space $\mathcal{V}_h^*$ anew and apply three distinct steps starting with the original *Eulerian space* $\mathcal{V}_h$.

Step 1 - Projection: Define the set of new nodes

$$\mathcal{X}_{h,\Gamma} := \mathcal{X}_h^* \setminus \mathcal{X}_h = \{x_k^*\}_{k\in\mathcal{I}_{h,\Gamma}}$$

as *Lagrangian points* (LP) of $\mathcal{T}_h$ with respect to Γ (see the blue vertices on Γ in Fig. 5a). The resulting discrete interface Γ_h defines a suitable projection of Γ onto the grid $\mathcal{T}_h$.

Step 2 - Embedding: For all $k \in \mathcal{I}_{h,\Gamma}$ define functions δ_k associated to each point $\mathbf{x}_k \in \mathcal{X}_{h,\Gamma}$ forming the *Lagrangian space* $\mathcal{L}_\Gamma := \operatorname{span}\{\delta_k\}_{k\in\mathcal{I}_{h,\Gamma}}$. For the sake of stability and consistency it is reasonable to embed the Lagrangian space $\mathcal{L}_\Gamma$ into an appropriate Eulerian (finite element) space with respect to $\mathcal{T}_h$. Since $\mathcal{X}_{h,\Gamma}$ is the set of intersections of Γ with the edges of triangles $T \in \mathcal{T}_h$, the definition

$$\delta_k(\mathbf{x}) := \varphi_k^*(\mathbf{x}) \in \mathcal{P}^k(\mathcal{T}_h^*),\ k \geq 1$$

yields a natural embedding $\mathcal{L}_\Gamma \subset \mathcal{V}_h^*$ into the enriched $\mathcal{V}_h^*$ which differs from the original space $\mathcal{V}_h$ only on cut elements.

Step 3 - Reduction: We request that the enriched space forms a *partition of unity* (PU) (see also Section 4, Remark 2). Therefore, the basis functions $\varphi_i \in \mathcal{V}_h$ in the near-interface nodes $\mathbf{x}_i \in \mathcal{X}_{h,\mathrm{Cut}}^j$, $j = 1, 2$, which share support with the functions δ_k, need to be projected onto corresponding shape functions with respect to the adapted mesh $\mathcal{T}_h^*$. We end up with *reduced* shape functions satisfying $\varphi_i^*(\mathbf{x})|_{\Omega_{j,h}} \equiv 0$ for all $i \notin \mathcal{I}_{h,\mathrm{Cut}}^j$, $j = 1, 2$, see Fig. 7a. We denote by $\mathcal{V}_h^- := \operatorname{span}\{\varphi_i^*\}_{i\notin\mathcal{I}_{h,\Gamma}}$ the *reduced Eulerian space* with respect to $\mathcal{T}_h$ and Γ. By means of the *Lagrangian* shape functions $\delta_k \in \mathcal{L}_\Gamma$ and the *reduced* shape functions $\varphi_i^* \in \mathcal{V}_h^-$ we finally define the *enriched* finite element space as the direct sum

$$\mathcal{V}_h^* = \mathcal{V}_h^- \oplus \mathcal{L}_\Gamma.$$

Remark that for the reduced space we in general obtain $\mathcal{V}_h^- \not\subset \mathcal{V}_h$ due to the bilinear cut elements.

Based on these three sub-steps we can compare our approach with two common immersed interface methods.

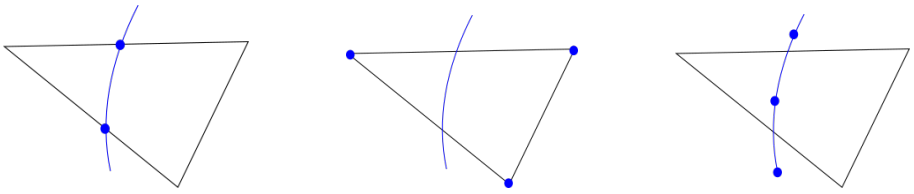

(a) projFEM: $\mathbf{x}_k^* \in \mathcal{X}_{h,\Gamma}$ (b) XFEM: $\mathbf{x}_i \in \mathcal{X}_h$ (c) DDF-IBM: $\mathbf{y}_i \in \Gamma$

Fig. 5: Newly defined nodes (blue) on a cut element: (a) projFEM: new DoFs $\mathbf{x}_k^*$ on the intersection of interface and edge. (b) XFEM: new DoFs $\mathbf{x}_i$ in the vertices across the interface (= doubling). (c) DDF-IBM: Nodes $\mathbf{y}_i$ equidistantly distributed along the interface.

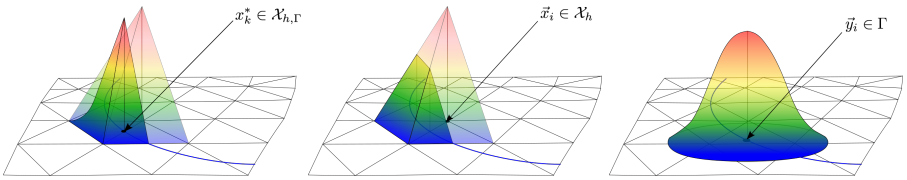

(a) projFVM: $\varphi_k^* \in \mathcal{L}_\Gamma \subset \mathcal{V}_h^*$. (b) XFEM: $\varphi_i \in \mathsf{R}_1(\mathcal{V}_h)$. (c) DDF-IBM: $\delta_i \in \mathcal{L}_\Gamma$.

Fig. 6: Different local spaces on a cut element: (a) projFEM/projFVM: Projected and embedded shape function φ_k^*. (b) XFEM: Extended and restricted shape function $\varphi_i|_{\Omega_{1,h}}$. (c) DDF-IBM: discrete delta function δ_i as force source.

3.1 XFEM: Embedding without reduction and projection

In the CutFEM approach of Hansbo and Hansbo [15] the discontinuity across Γ gets introduced into the local space of each cut element by *doubling* its degrees of freedom, see Fig. 5b. This is equivalent to extending each domain Ω_j across Γ - presuming the smoothness of the inner boundary. Subsequently, the two function spaces are restricted onto Ω_1 and Ω_2 which reconstructs the discontinuity. The doubling enables the retainment of the shape functions on the original mesh $\mathcal{T}_h$ and we obtain the locally extended space by

$$\mathcal{V}_h^{\text{ext}} := \mathsf{R}_1(\mathcal{V}_h) \oplus \mathsf{R}_2(\mathcal{V}_h),$$

with the according restriction operators $\mathsf{R}_j : L^2(\Omega) \to L^2(\Omega_j)$, $j = 1, 2$, see Fig. 6b. By construction, the space $\mathcal{V}_h^{\text{ext}}$ forms a PU, which is important to assure mass conservation, see Remark 2. However, the drawback of that construction is an asymmetry on the restricted elements $\mathsf{R}_j(T)$. Re-symmetrisation and stabilisation become necessary. Besides that, the gradient near the interface will remain unchanged independent of the location of the interface, see also Fig. 7b. For the detailed discussion of that observation we refer to Section 4.1.

3.2 DDF-IBM: Projection without embedding and reduction

In common DDF-IBM the unadapted discrete scheme is employed on the *background* Eulerian grid. In addition, LPs $\{\mathbf{y}_i\}_{i=1}^N$ are introduced, usually distributed equidistantly on the immersed boundary, see Fig. 5c, together with the associated *discrete delta functions* $\{\delta_i\}_{i=1}^N$, see Fig. 6c. Defining the Lagrangian space $\mathcal{L}_\Gamma := \text{span}\{\delta_i\}_{i=1}^N$ of all discrete delta functions we get a representation of the whole space as

$$\mathcal{V}_h^{\text{DDF}} := \mathcal{V}_h \times \mathcal{L}_\Gamma.$$

We want to emphasize that the LPs commonly do not serve as distinct degrees of freedom but as interpolation functions for prescribed forces which get distributed from the interface onto the Eulerian grid points. This technically yields $\mathcal{V}_h^{\text{DDF}} = \mathcal{V}_h$. Moreover, the discrete delta functions are not necessarily chosen in accordance with the shape functions on the Eulerian grid, i.e. $\delta_i \notin \mathcal{V}_h$. Most DDF-IBM approaches even do not define shape functions on the Eulerian grid since DDF-IBM is often applied for finite difference schemes on cartesian grids. The embedding into a common space is not intended. In addition, the set of functions $\mathcal{V}_h \times \mathcal{L}_\Gamma$ does mostly not form a PU. The DDF are defined to provide a good approximation of the forces rather than of the solution itself.

4 Properties of the Enriched Space

The projection and reduction step are the building blocks for the construction of $\mathcal{T}_h^*$ when deriving it from the originally given mesh $\mathcal{T}_h$. The direct consequence is the Kronecker-delta property of the enriching shape funcitons w.r.t. the interface. Its implications for the properties of the discrete scheme will be explained in the following.

Furthermore, the enriched spaces by construction form a partition of unity. In particular, projection and reduction are *mutually dependent* when claiming the partition of unity property, i.e. projection entails reduction and vice versa. The following remark emphasizes the importance of requesting partition of unity.

Remark 2 (Partition of Unity) The PU-property

$$\sum_{i \in \mathcal{I}_h^*} \varphi_i(\mathbf{x}) = 1 \qquad \forall \mathbf{x} \in \Omega$$

is a necessary and sufficient condition to guarantee mass conservation, see e.g. [23]. The standard finite element shape functions defined on the original mesh $\mathcal{T}_h$ satisfy the PU property. After the introduction of the shape functions in the projected LPs the reduction step becomes necessary in order to preserve the PU property.

4.1 The Kronecker-delta property: Consistency of the gradients

For application to particulate flows in [19] the construction of the enriched spaces by means of projection and reduction was driven by the requirement of consistent gradients of the shape functions near the interface. In the context of fluid problems directions of forces at the interface play a crucial role and these were shown to be related to the gradient of the test space. For more details we refer to [19].

4.2 The Kronecker-delta property: Natural stabilisation by steeper gradients

With regard to scalar elliptic problems we want to point out the impact of the projection and restriction on the stability. Since the enriched spaces can be interpreted as a special non-regular, interface-adapted refinement, the resulting finite element spaces are conforming. As a consequence, the formulation is based on the continuous bilinear form and inherits its nice properties: First, the symmetry is maintained and not impaired by additional penalisation terms. Second and more important, the stability of the bilinear operator can be easily guaranteed. In fact, for good approximation properties and conditioning the *shape regularity* of $\mathcal{T}_h^*$ is the only criterion that needs to be ensured, see Section 5.1. And in particular, small cut elements are not an issue. If the area of one part of the cut element is small, the small support of the shape function results in an almost-dependency between the degrees of freedom if the enrichment is based on shape functions w.r.t. to the original mesh. In contrast, $\mathcal{V}_h^*$ provides a natural stabilisation on small cut elements because of its gradients: For linear finite elements it is $|\nabla\varphi_i|_T = 1/h_i$ (with h_i being the height of T w.r.t. $\mathbf{x}_i$ and the opposite edge) and therefore they scale *inversely proportional* to the area of the element. For illustration, we consider the two dimensional case of a triangle $T \in \mathcal{T}_h$ of the original mesh. The local coupling matrix $A \in \mathbb{R}^{3\times 3}$, with $A_{ij} := a(\varphi_i, \varphi_j)$, is given as follows:

$$\begin{aligned} a(\varphi_i, \varphi_j) &= \int_T \nabla\varphi_i(x) \cdot \nabla\varphi_j(x)\, dx = |T|\, |\nabla\varphi_i(x)|\, |\nabla\varphi_j(x)|\, \cos(\alpha) \\ &= 0.5\, e_i/h_j\, \cos(\alpha). \end{aligned}$$

Considering the simplified case that the interface cuts the two edges of T in the same relation, i.e. $\Gamma_h \,||\, e_i$ for one $i \in \{1, 2, 3\}$. For the corresponding objects on the cut part $\tilde{T}$ this yields $\tilde{e}_i = \lambda e_i$ and $\tilde{h}_j = \lambda h_j$ for some $0 < \lambda < 1$. Hence, it is $\tilde{e}_i/\tilde{h}_i = e_i/h_i$ and $\tilde{A}_{ij} = A_{ij}$. Therefore, the condition of the matrix is not impaired because of small support. For the general case we still get $\tilde{A}_{ij} \approx A_{ij}$. Therefore, the *shape regularity* of a mesh is the only condition for the discrete system to be well-conditioned. A criterion for a suitable adaption of the scheme will be derived in Section 5.1.

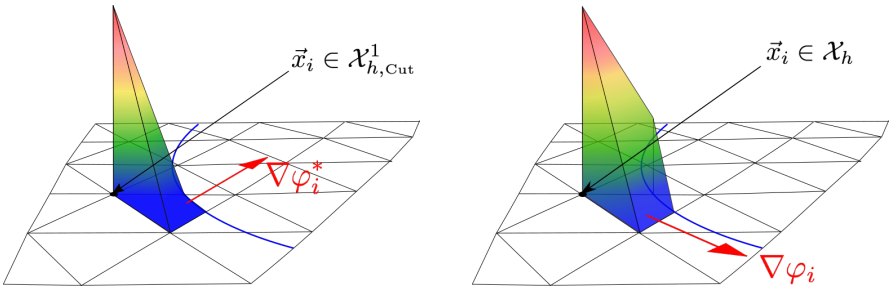

(a) Reduced shape fct $\varphi^*_i \in \mathcal{V}^-_h$. (b) Restricted shape fct $\varphi_i \in \mathsf{R}_1(\mathcal{V}_h)$.

Fig. 7: Shape functions for the *near-interface vertices* and its gradients (red arrow): (a) Reduced shape function with steeper gradients and pointing normal to the immersed interface; (b) Restricted shape function with unchanged gradient and pointing normal to the opposite edge of the according DoF.

4.3 Existence of a local finite element space on cut elements

Appropriate nodal shape functions for $\mathbf{x}^*_k \in \mathcal{X}_{h,\Gamma}$ with its support on the elements $T \in \mathcal{T}^j_{h,\mathrm{Cut}}$, $j = 1, 2$, need to be provided. For piecewise linear finite element spaces $\mathcal{V}_h := \mathcal{P}^1(\mathcal{T}_h)$ on simplicial triangulations suitable local spaces can be defined quite easily. In two dimensions the simplex is a triangle which gets cut into two triangles or a triangle and a quadrilateral (see Fig. 5a) on which correspondingly a linear and bi-linear ansatz exists, see Fig. 6a. In three dimensions the simplex is a tetrahedron and gets cut into combinations of tetrahedra, prisms and pyramids, see Fig. 8. For all these elements local shape functions of second order exist. The details on the local spaces used for our computations can be found in [32]. Consequently, for $T_j \in \mathcal{T}^j_{h,\mathrm{Cut}}$, $j = 1, 2$, we get the optimal approximation error [5]

$$\| \nabla^k (u - I_h u) \|_{0,T_j} \leq c\, h^{2-k}_{T_j} \| \nabla^2 u \|_{0,T_j}, \qquad k = 0, 1, \tag{12}$$

with constant $c > 0$ and h_{T_j} being half the diameter of the triangle T_j.
Our approach certainly will afford more effort for the definition of suitable local spaces on the cut elements, if the mesh contains also quadrilaterals or octahedrons in two or three dimensions, respectively. For all considered applications the simplicial grid was appropriate.

4.4 Cut elements as new reference elements

Because of the reduction step the discretisation w.r.t. the original mesh $\mathcal{T}_h$ can not be applied for the *near-interface* nodes. However, by the use of reference elements for the assembling process the usual assembling can be applied: Algorithms for finite element schemes on unstructured meshes usually exploit the

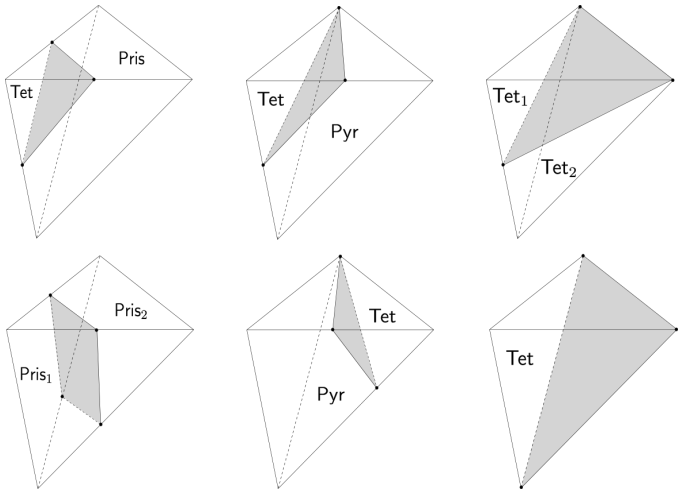

(a) No vertex on the interface; 3 edges (top) and 4 edges (bottom) cut by the interface.

(b) 1 vertex on the interface; 2 opposite edges cut by the interface.

(c) 2 vertices on the interface; opposite edge cut by the interface (top); 3 vertices on the interface (bottom).

Fig. 8: Different cut elements for $d = 3$: (a)-(c) categorization by the number of vertices and edges cut by the immersed interface.

possibility to map each (unstructured) element of the mesh onto a reference element. The assembling of the discrete system therefore depends solely on the coordinates of the corners of an element. With regard to Section 4.3 we can assume that for the sub-elements the discretisation on the reference element is well defined. As a consequence, the same standard routines for unstructured elements can be applied to the assembling on each cut element $T \in \mathcal{T}_{h,\mathrm{Cut}}$. This simply requires calling these routines twice and with respect to the corresponding new coordinates. Moreover, we maintain local stencils and optimal convergence properties as will be shown in Section 5.3. We emphasize, that in particular no special integration rules on the cut elements (due to e.g. restriction and change of support) need to be defined.

5 Numerical Analysis

In this section we will derive theoretical results for the projFEM in (6). Unfortunately, due to $\mathsf{R}(h) \neq 0$ for the space $\mathcal{V}_h^*$, the theoretical results can not directly be transferred to the projFVM in (8). However, since the enriched mesh $\mathcal{T}_h^*$ contains only a few multi-linear elements along the interface compared to the global number of elements, it is reasonable to assume that

$\mathsf{Rest}(h) = O(h^2)$ also holds for the projFVM, provided that $\mathcal{T}_h^*$ again is shape regular. We therefore already state for the projFVM in (8) that the results derived in the following subsections, based on finite element theory, together with the identification (11) at least allow us to expect a similar convergence behaviour for the projFVM. The numerical results presented in Section 6 apply the projFVM to elliptic problems and confirm our reasoning.

5.1 Conditioning

In the case of a moving interface the elements of $\mathcal{T}_h$ can be cut in arbitrary ways. Consequently, the shape-regularity of the mesh $\mathcal{T}_h^*$ is not guaranteed (i.e. the existence of a constant $\kappa > 0$ independent of the location of the interface, s.t. $h_T/\rho_T \leq \kappa$, with h_T and ρ_T being the circumcenter and incircle-radius of an arbitrary $T \in \mathcal{T}_h^*$). That is a potential source of ill-conditioning of our discrete scheme. In order to preserve shape-regularity we simply re-define those points $\mathbf{x}_k^* \in \mathcal{X}_{h,\Gamma}$ whose distance to a point on the Eulerian mesh falls below a certain threshold. This way, also the approximation property will not be impaired. To formulate a suitable criterion for a re-definition we choose a lower bound $D > 0$ satisfying $D < h_{\min}$, with $h_{\min} := \min\{h_T : T \in \mathcal{T}_h\}$ being the minimal circumcenter in the original grid. The re-definition then reads:

$$\forall k \in \mathcal{I}_{h,\Gamma}: \text{ If } \quad d_{i,k} := |\mathbf{x}_i - \mathbf{x}_k^*| \leq D \quad \text{for} \quad \mathbf{x}_i \in \mathcal{T}_h, \quad \text{re-define } \mathbf{x}_k^* := \mathbf{x}_i. \tag{13}$$

The adapted triangulation $\mathcal{T}_h^*$ satisfies the condition $h_T/\kappa \leq \rho_T$. The proof can be found in [18]. The resulting discrete interface Γ_h approximates Γ less accurately. However, for the choice of $D := h^2 < h_{\min}$, with h being the mean circumcenter of the given grid, we can conclude that the resulting piecewise planar interface Γ_h satisfies

$$\operatorname{dist}(\Gamma_h, \Gamma) \leq c\, h^2. \tag{14}$$

In Section 5.3 we will show that the corresponding discrete scheme maintains optimal approximation order. A higher condition number in favor of a stable solution process for the linear system appears to be a valid strategy confirmed by the numerical simulations in Section 6.

In common XFEM approaches the ill-conditioning of the discrete system is similarly an issue. But in contrast to the shape-regularity above, already small but shape-regular cut elements are critical, see Section 4.2. There we also explained that the stabilising effect of the steeper gradients of the projected and reduced shape functions (which in particular are not defined w.r.t. the original mesh). The *Hansbo-averageing* is a general strategy to handle the issue of ill-conditioning due to small support for the CutFEM spaces. We want to mention it in order to contrast it to the proposed re-definition in (13):

Remark 3 (Hansbo-averageing) Formulations based on Nitsche's method [27] introduce an averaging operator $\{\cdot\}$ to re-weight the shape functions on the

cut elements by

$$\{\varphi\} := (\kappa_1\varphi_1 + \kappa_2\varphi_2)|_\Gamma, \quad \varphi_j \in \mathsf{R}_j(\mathcal{V}_h), \tag{15}$$

with weights κ_1 and κ_2 satisfying $\kappa_1 + \kappa_2 = 1$ in order to preserve consistency of the discrete scheme. For $T_j := \mathrm{supp}(\varphi_j) \cap T$, $j = 1, 2$, the so called *Hansbo-averaging*, cf. [15], defines $\kappa_j := T_j/T$. Hence, the weights depend on the size of the relative area of each sub-element which resembles the parameter $d_{i,j}$ in (13). Other weighting strategies are defined in [17], [29], [33] likewise depending on the properties of the sub-elements.

Remark 4 (Neglection vs. Redefinition) A weighting rule which defines $\kappa_1 := 0$ and $\kappa_2 := 1$ in (15) in the case of very small support, i.e. $T_1/T \approx 0$, corresponds to neglecting the presence of the interface on the cut element T. Optimal approximation of the solution can be preserved if a criterion for neglecting is defined suitably, cf. [29]. It should be emphasized that the described re-definition in (13) resembles the strategy of neglecting but does *not* correspond to it: Consider the case of a two-dimensional triangle cut by the interface in such a way that after application of criterion (13) the whole triangle lies on one side of the interface. Therefore, the triangle will not be part of the enrichment. In contrast to neglecting the interface, the re-definition of the LP leads to a slight displacement of the interface. In particular, also on the neighbouring elements the shape of Γ_h gets displaced. The essential consequence is the continuity of the interface across neighbouring cut elements.

5.2 Coercivity and Symmetry

The coercivity of $a_{\mathrm{FE}}(\cdot,\cdot)$ on $\mathcal{V}_h^*$ directly follows from the coercivity of the continuous bilinear form. That directly implies the important advantage of our approach that no additional stabilisation is needed which can cause numerical fluxes across the interface. With regard to the coercivity of $a_{\mathrm{FV}}(\cdot,\cdot)$ on $\mathcal{V}_h^*$, we state the following:

Remark 5 (Coercivity of $a_{FV}(\cdot,\cdot)$) Due to (11) the coercivity of the finite volume scheme is potentially impaired only on the multi-linear elements. Based on our assumption that $\mathsf{Rest}(h) = O(h^2)$ there exists a $h_{\mathrm{FV}} > 0$ and an according constant $C(h_{\mathrm{FV}})$ such that the coercivity is satisfied with constant $C(h_{\mathrm{FV}})$ and for all $h \leq h_{\mathrm{FV}}$.

A further advantage of the proposed projFEM and projFVM is the avoidance of the weak boundary condition term $([\alpha\nabla u \cdot \mathbf{n}], v)_\Gamma$ so that the symmetry of the scheme is preserved. Since the original problem is self-adjoint, the lack of symmetry and therefore adjoint-consistency can lead to impaired numerical results. For that reason Nitsche's method retrieves symmetry by introducing suitable additional terms.

5.3 A Priori Error Analysis

In order to derive an a priori error estimate for problem (5) we in particular need to bound the approximation error. The shape-regularity is guaranteed by means of 13. This enables to use the standard nodal interpolation operator $I_h : H^2(\Omega) \to \mathcal{V}_h^*$ w.r.t. $\mathcal{T}_h^*$, i.e. $(I_h u)(x_k) = u(x_k)$ for all $x_k \in \mathcal{X}_h^*$. For all elements $T \notin \mathcal{T}_{h,\mathrm{Cut}}$ being *not* cut by the interface, we get the optimal approximation error [5]

$$\| \nabla^k (u - I_h u) \|_{0,T} \leq C\, h_T^{2-k} \| \nabla^2 u \|_{0,T}, \qquad k = 0, 1, \tag{16}$$

with constant $C > 0$ and h_T being half the diameter of the triangle T, see also (12).

For a complete a priori analysis two difficulties need to be addressed: the solution u is not smooth across the interface Γ and due to $\Gamma_h \not\subset \Gamma$ the piecewise linear, discrete interface is not aligned with the real interface. It is therefore necessary to derive appropriate interpolation estimates on the according elements $T \in \mathcal{T}_{h,\mathrm{Cut}}$.

Lemma 1 (Interpolation Error on $\mathcal{T}_h^*$) *Let $\Omega := \Omega_1 \cup \Omega_2 \cup \Gamma \subset \mathbb{R}^d$ be a polygonal and convex domain with embedded smooth interface $\Gamma = \partial\Omega_1 \cap \partial\Omega_2$. Let further $I_h : H^2(\Omega) \to \mathcal{V}_h^*$ be the standard nodal interpolation operator w.r.t. $\mathcal{T}^*$. For all $u \in H^2(\Omega_{1,2})$ it holds that*

$$\| \nabla (u - I_h u) \|_{0,\Omega} \leq Ch \| u \|_{2,\Omega_1 \cup \Omega_2}.$$

Proof Let $T_c \in \mathcal{T}_{h,\mathrm{Cut}}$. By means of 16 it is sufficient to derive an estimate for $\| \nabla (u - I_h u) \|_{0,T_c}$. The proof is based on the reasoning in the work of Frei and Richter [11], Frei [10] and Basting and Prignitz [2]. Their proofs rely on a continuous extension $\tilde{u}_i \in H^2(\Omega)$ of $u \in H^2(\Omega_i)$, $i = 1, 2$. Such an extension exists, see [34] and satisfies

$$\| u - \tilde{u}_i \|_{2,\Omega_i} = 0, \qquad \|\tilde{u}_i\|_{2,\Omega} \leq C \|u\|_{2,\Omega_i}. \tag{17}$$

Insertion of $\pm\, \tilde{u}_i$ and $\pm\, I_h \tilde{u}_i$ yields

$$\| \nabla (u - I_h u) \|_{0,T_c} \leq \| \nabla (u - \tilde{u}_i) \|_{0,T_c} + \| \nabla (\tilde{u}_i - I_h \tilde{u}_i) \|_{0,T_c}. \tag{18}$$

Since all Lagrange nodes lie on the interface, it is $I_h \tilde{u}_i = I_h u$ and therefore the according term of the insertion vanishes. To derive an estimate for $\| \nabla (u - \tilde{u}_i) \|_{0,T_c}$ we can apply the same argumentation as in [11], [10]. Herein, they use a Poincare-like estimate to bound $\| \nabla u \|_{0,T_c}$. Combined with the continuity of the extension (17) this yields [11], [10]

$$\| \nabla (u - \tilde{u}_i) \|_{0,T_c} \leq \| \nabla u \|_{0,T_c} + \| \nabla \tilde{u}_i \|_{0,T_c} \leq Ch \|u\|_{2,\Omega_1 \cup \Omega_2}. \tag{19}$$

To derive an estimate for the interpolation error $\| \nabla (\tilde{u}_i - I_h \tilde{u}_i) \|_{0,T_c}$ we can use the standard estimate stated in (12), since it is $T_c = T_1 \cup T_2$, with $T_1 \in \mathcal{T}_{h,\mathrm{Cut}}^1$,

$T_2 \in \mathcal{T}^2_{h,\mathrm{Cut}}$. Together with an enlargement onto Ω and again the continuity of the extension (17) we get

$$\| \nabla(\tilde{u}_i - I_h\tilde{u}_i) \|_{0,T_c} \leq Ch \| \nabla^2\tilde{u}_i \|_{0,T_c} \leq Ch \| \nabla^2\tilde{u}_i \|_{0,\Omega} \leq Ch \| \nabla^2 u \|_{0,\Omega_i}.$$

Combining the last estimate with (18) and (19) completes the proof.

The final discretisation error bound can be derived by combining the interpolation error stated in Lemma 1 with the consistency error. That is the common procedure in Strang's lemmata. Let $u \in H^2(\Omega_{1,2})$ and $u_h \in \mathcal{V}_h^*$ be solutions of problem (5) and (6), respectively. For arbitrary, but fixed coefficients α_1 and α_2 let further c_α be the according coercivity constant, i.e.

$$a_{\mathrm{FE}}(v_h, v_h) \geq c_\alpha \|v_h\|^2_{1,\Omega} \qquad \forall v_h \in \mathcal{V}_h^*,$$

with $c_\alpha > 0$ being independent of h. Application of Strang's first lemma directly yields the following estimate for the discretisation error:

$$\| u - u_h \|_{1,\Omega} \leq (1 + \frac{c_c}{c_\alpha}) \inf_{v_h \in \mathcal{V}_h^*} \| u - v_h \|_{1,\Omega} \tag{20}$$

$$+ \frac{c_c}{c_\alpha} \sup_{w_h \in \mathcal{V}_h^*} \frac{| a(v_h, w_h) - a_{\mathrm{FE}}(v_h, w_h) |}{\| w_h \|_{1,\Omega}} \tag{21}$$

$$+ \frac{c_c}{c_\alpha} \sup_{w_h \in \mathcal{V}_h^*} \frac{| l(w_h) - l_{\mathrm{FE}}(w_h) |}{\| w_h \|_{1,\Omega}}, \tag{22}$$

with continuity constant $c_c > 0$ being indepentend of h, $l(w_h) = (f, w_h) + (g, w_h)_\Gamma$ and $l_{\mathrm{FE}}(w_h) = (f_h, w_h) + (g, w_h)_\Gamma$. An appropriate definition of f_h yields an $O(h)$ error bound of the term in (22). In order to proof Theorem 1 it remains to bound the consistency error in (21) due to the difference between the continuous and discrete bilinear forms

$$\big| a(v_h, w_h) - a_{\mathrm{FE}}(v_h, w_h) \big| = \big| \left((\alpha - \alpha_h) \nabla v_h, \nabla w_h \right) \big|.$$

We state the following optimal approximation error bound:

Theorem 1 *Let $u \in H^2(\Omega_{1,2})$ and $u_h \in \mathcal{V}_h^*$ be the solution of problem (5) and (6), respectively. Then the a priori error estimate*

$$\| u - u_h \|_{1,\Omega} \leq Ch \| u \|_{2,\Omega_1 \cup \Omega_2} \tag{23}$$

holds with constant C independent of h.

Proof Remark that $| a(v_h, w_h) - a_{\mathrm{FE}}(v_h, w_h) |$ vanishes on $\Omega_j \cap \Omega_{j,h}$, $j = 1, 2$. The relevant region is the one, which gets *cut off* by the linearized interface Γ_h. We shell denote this region by $O_{1,2}$, since it is *overlapping* either with Ω_1 or with Ω_2. From (14) we obtain $| O_{1,2} | = O(h^2)$, $j = 1, 2$, see also [29], [2]. Since $\mathcal{T}_{h,\mathrm{Cut}}$ contains all cut elements $T_c = T_1 \cup T_2$, which are not yet devided

into its two pieces, it is $O_{1,2} \subset \mathcal{T}_{h,\mathrm{Cut}}$ and $|\,\mathcal{T}_{h,\mathrm{Cut}}\,| = O(h)$. Since the gradient $\nabla\phi_h$ is piecewise constant for $\phi_h \in \mathcal{V}_h^*$, we directly get

$$\| \nabla\phi_h \|_{0,O_{1,2}}^2 \leq Ch \| \nabla\phi_h \|_{0,\mathcal{T}_{h,\mathrm{Cut}}}^2.$$

We finally get the estimate

$$\begin{aligned} |\, a(v_h, w_h) - a_{\mathrm{FE}}(v_h, w_h) \,| &= \Big| \int_{O_{1,2}} (\alpha(\mathbf{x}) - \alpha_h(\mathbf{x})\,) \nabla v_h \cdot \nabla w_h \, d\mathbf{x} \Big| \\ &\leq Ch \| \nabla v_h \|_{0,\Omega_1\cup\Omega_2} \| \nabla w_h \|_{0,\Omega_1\cup\Omega_2}, \end{aligned}$$

for all v_h, $w_h \in \mathcal{V}_h^*$. Combined with the estimate in Lemma 1 this yields (23).

In the work of Frei and Richter [11], Frei [10] and Basting and Prignitz [2] slightly different discrete spaces are suggested, where they similarly introduce Lagrange nodes on the interface and derive the same error estimates. Furthermore, for the CutFEM spaces, comparable approximation error bounds have been derived in Reusken [29] and Hansbo and Hansbo [15].

6 Numerical Experiments

In this section we apply the projFVM introduced in Section 2 to the problem (1)-(4) for different test cases.

6.1 Experiment 1

This test case was already investigated by Liu et al. [24]. The computational domain is the unit square $\Omega = (-1, 1)^2$ and the interface Γ is defined as the circle with radius $R = 0.5$ and center $\mathbf{x}_m = (0.0, 0.0)$. As diffusion coefficients we choose $\alpha_1 = \alpha_2 = 1$. The analytical solution for $\Delta u = 0$ is given by

$$u(\mathbf{x}) = \begin{cases} 1 + \ln(2\,||\mathbf{x}||) & \mathbf{x} \in \Omega_1, \\ 1 & \mathbf{x} \in \Omega_2. \end{cases} \tag{24}$$

The Dirichlet data is defined according to the exact solution $u(\mathbf{x})$ yielding the non-zero jump condition $g(\mathbf{x}) = 2$.

The L^2-errors obtained under global mesh refinement are depicted in Figure 9a. We get a convergence of order $O(h^2)$ in accordance with Theorem 1.

n	h	$\|u-u_h\|_2$	rate L_2
289	h_0	6.230e-03	—
1089	$h_0/2$	1.683e-03	1.89
4467	$h_0/4$	4.144e-04	2.02
16641	$h_0/8$	1.039e-04	1.99
66049	$h_0/16$	2.635e-05	1.98
263169	$h_0/32$	6.598e-06	1.99

(a) Computed L^2-error.

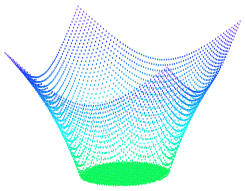

(b) Sketch of the solution.

Fig. 9: Second order convergence for the interface problem (24).

6.2 Experiment 2

This test case was already investigated with variations by Frei and Richter [11] and Gangl and Langer [12]. The computational domain is the unit square $\Omega = (-1,1)^2$ and the interface Γ is defined as the circle with radius $R = 0.4$ and center $\mathbf{x}_m = (0.0, 0.0)$. As diffusion coefficients we choose $\alpha_1 = 10$ and $\alpha_2 = 1$. The analytical solution is given by

$$u(\mathbf{x}) = \begin{cases} -2\alpha_1 ||\mathbf{x}-\mathbf{x}_m||^4 & \mathbf{x} \in \Omega_1, \\ -4\alpha_1\alpha_2^2 R^2 ||\mathbf{x}-\mathbf{x}_m||^2 + 2R^4\alpha_1(2\alpha_2\alpha_1 - 1) & \mathbf{x} \in \Omega_2. \end{cases} \tag{25}$$

The right hand side and the Dirichlet data are defined according to the exact solution $u(\mathbf{x})$. Remark that the weak discontinuity in the solution along Γ combined with the jumping coefficients yield a jump condition equal to zero, i.e. $g(\mathbf{x}) = 0$.

The L^2-errors obtained under global mesh refinement are depicted in Figure 10a. We get a convergence of order $O(h^2)$ in accordance with Theorem 1.

The same experiment was performed with shifted center $\mathbf{x}_m = (-0.08, 0.3)$

n	h	$\|u-u_h\|_2$	rate L_2
289	h_0	1.575e-00	—
1089	$h_0/2$	4.107e-01	1.94
4467	$h_0/4$	1.125e-01	1.87
16641	$h_0/8$	2.377e-02	2.24
66049	$h_0/16$	5.945e-03	1.99
263169	$h_0/32$	1.488e-03	1.99

(a) Computed L^2-error.

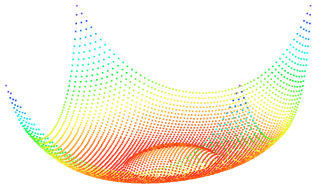

(b) Sketch of the solution.

Fig. 10: Second order convergence for the interface problem (25) and $\mathbf{x}_m = (0.0, 0.0)$.

n	h	$\|u - u_h\|_2$	rate L_2
289	h_0	1.737e-00	—
1089	$h_0/2$	3.962e-01	2.13
4467	$h_0/4$	1.054e-01	1.91
16641	$h_0/8$	2.491e-02	2.08
66049	$h_0/16$	7.033e-03	1.82
263169	$h_0/32$	1.789e-03	1.98

(a) Computed L^2-error.

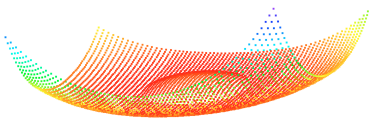

(b) Sketch of the solution.

Fig. 11: Second order convergence for the interface problem (25) and $\mathbf{x}_m = (-0.08, 0.3)$.

and same radius $R = 0.4$. A comparable L^2-error was obtained and is depicted in Figure 11a.

7 Conclusions

We proposed enriched finite element spaces which yield an interface fitted scheme for elliptic interface problems. Therefore, the derived method provides the advantage of an immersed interface method avoiding costy remeshing. In [19] the enrichment was derived for particulate flows. The motivation was a correct discretisation of the forces acting on the boundary. Therein, the focus was the gradient of the enriching shape functions. In this paper we could show that applied to a general elliptic interface problem we get the same order of approximation as comparable enriched methods. But in contrast to those, the discrete operator even herits the symmetry and positive definiteness of the continuous operator since it is a fitted method.

We further compared our method with the enrichment of a CutFEM and the idea of Peskins original IBM by looking at the local finite element spaces used in the according approach. Instead of extending and restricting the domain at the interface for the CutFEM, we apply as we call it projection and reduction. By opposing the shape functions on cut elements we could argue, that as already for the application in [19] the gradient of the enriching shape functions has a crucial role. Its slight change depicted in Figures 6 and 7 inherits a natural stabilisation on small cut elements.

In summary, a deeper insight into the properties of the enriching shape functions could provide a physically meaningful formulation of the interface problem with good numerical properties and without the need for additional, usually non-physical penalty terms.

In the case of deformable interfaces a good approximation of an immersed interface and the forces due to gradients becomes even more relevant. Therefore, the next step will be the application of the derived approach to multiphase flows.

Acknowledgements

The authors are grateful to D. Logaschenko for the useful discussions.

References

1. Bank RE, Rose DJ (1987) Some Error Estimates for the Box Method. SIAM Journal on Numerical Analysis 24:777–787
2. Basting S, Prignitz R (2013) An interface-fitted subspace projection method for finite element simulations of particulate flows. Comput Methods Appl Mech Engrg 267:133–149
3. Becker R, Burman E, Hansbo P (2009) A Nitsche extended finite element method for incompressible elasticity with discontinuous modulus of elasticity. Computer Methods in Applied Mechanics and Engineering 198:3352–3360
4. Bey J (1997) Finite-Volumen- und Mehrgitterverfahren für elliptische Randwertprobleme. PhD thesis, Universität Tübingen
5. Braess D (2007) Finite Elemente. Springer-Verlag Berlin Heidelberg
6. Burman E, Fernandez MA (2009) Stabilization of explicit coupling in fluid-structure interaction involving fluid incompressibility. Computer Methods in Applied Mechanics and Engineering 198(5-8):766–784
7. Burman E, Hansbo P, Larson MG, Massing A (2017) A cut discontinuous Galerkin method for the Laplace-Beltrami operator. AIMA Journal of Numerical Analysis 37:138–169
8. Chen L (2010) Finite Volume Methods. private Communication Http://www.math.uci.edu/∼chenlong/226/FVM.pdf
9. Chou S, Kwak DY (1997) Analysis and Convergence of a MAC-like Scheme for the Generalized Stokes Problem. Numerical Methods for Partial Differential Equations 13:147–162
10. Frei S (2016) Eulerian finite element methods for interface problems and fluid-structure interactions. PhD thesis, Heidelberg University, http://www.ub.uni-heidelberg.de/archiv/21590
11. Frei S, Richter T (2014) A locally modified parametric finite element method for interface problems. SIAM Journal on Numerical Analysis 52:2315–2334
12. Gangl P, Langer U (2018) A Local Mesh Modification Strategy for Interface Problems with Application to Shape and Topology Optimization. Scientific Computing in Electrical Engineering Mathematics in Industry 28:147–155
13. Gross S, Ludescher T, Olshanskii M, Reusken A (2016) Robust Preconditioning for XFEM Applied to Time-Dependent Stokes Problems. SIAM Journal of Scientific Computing 38(6):A3492–A3514
14. Hackbusch W (1989) On First and Second Order Box Schemes. Computing 41(4):277–296

15. Hansbo A, Hansbo P (2002) An unfitted finite element method, based on Nitsche's method, for elliptic interface problems. Computer Methods in Applied Mechanics and Engineering 191(47-48):5537–5552
16. Hansbo P, Hermansson J, Svedberg T (2004) Nitsche's method combined with space-time finite elements for ALE fluid-structure interaction problems. Computer Methods in Applied Mechanics and Engineering 193(39-41 SPEC. ISS.):4195–4206
17. Hansbo P, Larson MG, Zahedi S (2014) A cut finite element method for a Stokes interface problem. Applied Numerical Mathematics 85:90–114
18. Höllbacher S (2016) Voll gekoppelte Modellierung zur direkten numerischen Simulation partikulärer Fluide. PhD thesis, Universität Frankfurt
19. Höllbacher S, Wittum G (2019) Gradient-consistent enrichment of finite element spaces for the DNS of fluid-particle interaction. TBA
20. Höllbacher S, Wittum G (2019) Rotational test spaces for a fully-implicit FVM and FEM for DNS of fluid-particle interaction. Journal of Computational Physics 393:186–213
21. I Babuska UB, Osborn JE (2004) Generalized finite element methods: Main ideas, results, and perspective. Int J Comput Methods 1:67–103
22. Kirchhart M, Gross S, Reusken A (2017) Analysis of an XFEM Discretization for Stokes Interface Problems. SIAM Journal of Scientific Computing 38(2):A1019–A1043
23. Liu CR (2016) On Partitions of Unity Property of Nodal Shape Functions: Rigid-Body-Movement Reproduction and Mass Conservation. International Journal of Computational Methods 13:1–13
24. Liu XD, Fedkiw RP, Kang M (2000) A Boundary Condition Capturing Method for Poissons Equation on Irregular Domains. Journal of Computational Physics 160:151–178
25. Mittal R, Iaccarino G (2005) Immersed Boundary Methods. Annual Review of Fluid Mechanics 37(1):239–261
26. Moës N, Dolbow J, Belytschko T (1999) A finite element method for crack growth without remeshing. International Journal for Numerical Methods in Engineering 46:131–150
27. Nitsche J (1971) Über ein Variationsprinzip zur Lösung von Dirichlet-Problemen bei Verwendung von Teilräumen, die keinen Randbedingungen unterworfen sind. Abh ad Math Sem Univ Hamburg 36:9–15
28. Peskin CS (1977) Numerical Analysis of Blood Flow in the Heart. Journal of Computational Physics 25:220–252
29. Reusken A (2008) Analysis of an extended pressure finite element space for two-phase incompressible flows. Computing and Visualization in Science 11(4-6):293–305
30. Tornberg TK, Engquist B (2003) Regularization techniques for numerical approximation of PDES with singularities. Journal of Scientific Computing 19:527–552
31. Tornberg TK, Engquist B (2004) Numerical approximations of singular source terms in differential equations. Journal of Computational Physics

200:462–488
32. Vogel A, Reiter S, Rupp M, Nägel A, Wittum G (2013) UG 4: A novel flexible software system for simulating PDE based models on high performance computers. Computing and Visualization in Science 16:165–179
33. Wang F, Xiao Y, Xu J (2016) High-Order Extended Finite Element Methods for Solving Interface Problems. Numerical Analysis pp 1–25, 1604.06171
34. Wloka J (1982) Partielle Differentialgleichungen. Teubner, Stuttgart
35. Xu J, Zou Q (2009) Analysis of linear and quadratic simplicial finite volume methods for elliptic equations. Numerische Mathematik 111(3):469–492
36. Ye X (2001) On the Relationship Between Finite Volume and Finite Element Methods Applied to the Stokes Equations. Numerical Methods for Partial Differential Equations 17:440–453